PNAS RESEARCH ARTICLE | PHYSICS

Mechanism of superconductivity in the Hubbard model at intermediate interaction strength

Xinyang Dong[a,1], Lorenzo Del Re[b,c], Alessandro Toschi[d], and Emanuel Gull[a,1]

Edited by Douglas J. Scalapino, University of California, Santa Barbara, CA; received March 23, 2022; accepted July 1, 2022

We study the fluctuations responsible for pairing in the d-wave superconducting state of the two-dimensional Hubbard model at intermediate coupling within a cluster dynamical mean-field theory with a numerically exact quantum impurity solver. By analyzing how momentum- and frequency-dependent fluctuations generate the d-wave superconducting state in different representations, we identify antiferromagnetic fluctuations as the pairing glue of superconductivity in both the underdoped and the overdoped regime. Nevertheless, in the intermediate coupling regime, the predominant magnetic fluctuations may differ significantly from those described by conventional spin fluctuation theory.

Superconductivity | Strongly correlated system | Spin fluctuation theory

Significance

We investigate the pairing glue of superconductivity in the two-dimensional Hubbard model, for interaction values relevant to cuprate physics, within a nonperturbative and unbiased approach. In a generalized fluctuation diagnostics scheme applied to the ordered superconducting state, we analyze the self-energies and scattering amplitudes computed by means of cluster dynamical mean-field theory below the critical temperature of superconductivity. Independent of the doping level, we rigorously identify antiferromagnetic fluctuations as the dominant mechanism driving the unconventional d-wave superconducting phase. These fluctuations are of a different nature from those considered in traditional spin fluctuation approximations.

The microscopic mechanism of unconventional high-temperature superconductivity has been one of the most controversially debated topics in condensed matter physics since the discovery of superconductivity in layered copper-oxides in 1986. While several aspects of the observed physics, such as the d-wave symmetry of the order parameter and the proximity to an antiferromagnetic Mott phase, clearly suggest that superconductivity must emerge from strongly correlated electronic processes, the intrinsic quantum many-body nature of the problem has hitherto prevented a rigorous identification of the pairing glue. To explicitly address this point, we present a focused study of the origin of superconductivity in the two-dimensional single-band Hubbard model. The Hubbard Hamiltonian, which includes a kinetic term describing the hopping between neighboring sites on a lattice and a potential energy term encoding a local electrostatic repulsion, is a minimal theoretical model believed to capture the salient aspects of cuprate superconductivity.

Among the theoretical explanations proposed for the origin of the high-temperature superconductivity in this context, spin fluctuations have been a prominent scenario since the beginning (1–4). In particular, within the weak-coupling regime of the Hubbard model, renormalization group techniques (5–8) find d-wave superconductivity in qualitative agreement with spin fluctuation exchange studies (1, 8), consistent with diagrammatic Monte Carlo calculations (9). At the same time, other qualitatively different microscopic pictures of superconductivity exist besides the spin fluctuations, including the resonating valence bond theory (10), nematic fluctuations (11), loop current order (12), or the intertwining of orders of different types (13). In fact, to what extent the weak-coupling spin fluctuation results apply to the much stronger interaction values, which are typical of cuprate materials, and whether there are other competing or intertwining fluctuations driving the superconductivity remain unresolved.

To provide a conclusive answer, we perform an analysis of the anomalous self-energy in the d-wave superconducting state within the method of fluctuation diagnostics (14). We note that unlike other diagrammatic approaches, which postulate a specific physical mechanism, analyze its consequences, and then compare to experiments, the fluctuation diagnostics procedure treats fluctuations of all kinds, including those possibly driving superconductivity, on equal footing and is applicable in all parameter regimes, independent of the degree of correlation. However, the fluctuation diagnostics procedure as derived in ref. 14 was only applicable to the highly symmetric normal state and thus cannot be used to analyze superconductivity. Hence, we will first generalize this approach to the case of phases with spontaneously broken symmetries and then apply it to identify the dominant fluctuations driving the anomalous self-energy in the superconducting state.

Method

The Hamiltonian of the two-dimensional single band Hubbard model is

$$H = \sum_{k\sigma} (\varepsilon_k - \mu) c^\dagger_{k\sigma} c_{k\sigma} + U \sum_i n_{i\uparrow} n_{i\downarrow}, \qquad [1]$$

Author affiliations: [a]Department of Physics, University of Michigan, Ann Arbor, MI 48109; [b]Department of Physics, Georgetown University, Washington, DC 20057; [c]Correlated Phases in Quantum Materials Research Group, Max Planck Institute for Solid State Research, D-70569 Stuttgart, Germany; and [d]Institute of Solid State Physics, Technische Universität Wien, 1040 Vienna, Austria

Author contributions: A.T. and E.G. designed research; X.D., L.D.R., A.T., and E.G. performed research; X.D. and E.G. contributed new reagents/analytic tools; X.D., L.D.R., A.T., and E.G. analyzed data; and X.D., L.D.R., A.T., and E.G. wrote the paper.

The authors declare no competing interest.

This article is a PNAS Direct Submission.

[1]To whom correspondence may be addressed. Email: dongxy@umich.edu or egull@umich.edu.

Published August 10, 2022.

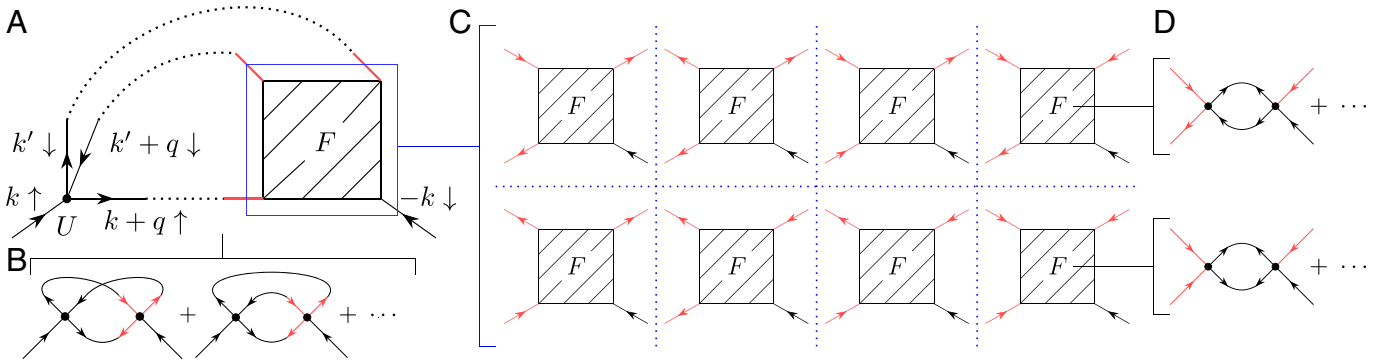

Fig. 1. Anomalous self-energy diagrams. (*A*) SD equation (Eq. **2**). Shaded box denotes vertex F with one fixed outgoing leg. Dotted lines indicate normal or anomalous Green's function. (*B*) Low-order anomalous self-energy diagrams. (*C*) Explicit representation of index combinations of F. (*D*) Some of the low-order diagrams contributing to F.

with i being a lattice site, k being momentum, $c^{(\dagger)}$ being annihilation (creation) operators, and n being the density. $\varepsilon_k = -2t(\cos k_x + \cos k_y)$ is the dispersion with hopping t, U is the interaction strength, and μ is the chemical potential. We use the dynamical cluster approximation (DCA) (15) on a cluster with size $N_c = 8$ with a numerically exact continuous time auxiliary field (16, 17) impurity solver to enter the superconducting state nonperturbatively (18) and obtain Green's functions, self-energies, and vertex functions.

In the DCA, the momentum structure of the Hubbard model self-energy is approximated by N_c basis functions which retain the full frequency dependence (15). To enter the superconducting phase, we allow for order and provide a superconducting bias field at the first iteration, removing it in subsequent iterations to converge to the equilibrium state. Within the eight-site DCA approximation, the model exhibits a large and stable d-wave superconducting region (18, 19). The model is known to also exhibit a stripe phase (20–24), to which our calculation is not sensitive, since its periodicity is larger than the $N_c = 8$ cluster. Recent accurate calculations on different system geometries (22) find that the ground state of the model is charge ordered, rather than superconducting, indicating that the state found by DCA may be competing with a stripe state nearby in energy. Based on the closeness of the energetics, it is reasonable to assume that both states are important (25) and that one or the other will be selected based on minor variations of system geometries, approximations, and model parameters.

To identify the superconducting glue, we apply the fluctuation diagnostics scheme (14) to the anomalous self-energy in the superconducting state. This approach, which so far has been derived (14) and applied (14, 26, 27) only in the paramagnetic normal state, allows for a rigorous identification of the dominant scattering mechanisms responsible for the observed self-energy. Fluctuation diagnostics exploits symmetries in the Hamiltonian that lead to different expressions for the Schwinger-Dyson (SD) equation of the self-energy Σ

$$\Sigma(18) - \Sigma_\infty = -U(1234)G(25)F(5678)G(63)G(74), \qquad [2]$$

where we have used the Einstein summation notation and introduced the shorthand notation $i = (K_i, \sigma_i, \tau_i)$ for momentum, spin, and time indices. The two indices on the self-energy $\Sigma(12)$ and the Green's functions $G(12)$ represent their normal ($1 = 2$) and anomalous ($1 = -2$) components, with $-i = (-K_i, -\sigma_i, \tau_i)$. Σ_∞ is the static Hartree contribution for the normal self-energy, and F is the full two-electron scattering amplitude. $U(1234)$ denotes the antisymmetrized interaction which, in the Hubbard model, is proportional to the local interaction U. This expression is exact and relates two-particle fluctuations to single-particle quantities.

Fig. 1*A* shows a diagrammatic representation of the anomalous self-energy of Eq. **2** in frequency space, with $k = (K, i\omega_n)$ representing fermionic and $q = (Q, i\nu_n)$ representing bosonic indices. A choice of $k_1 = k, \sigma_1 = \uparrow, k_2 = k + q, \sigma_2 = \uparrow, k_3 = k' + q, \sigma_3 = \downarrow, k_4 = k', \sigma_4 = \downarrow$, and $k_8 = -k, \sigma_8 = \downarrow$ satisfies momentum, energy, and spin conservations. Fig. 1*B* shows two low-order terms. F, in the case of superconducting order, can have eight possible combinations of incoming or outgoing legs, as illustrated in Fig. 1*C*. It then contains all allowed scattering processes, some of which are illustrated in Fig. 1*D*.

As F contains all fluctuations of the system, the different expressions of the SD are equivalent when all internal summations are performed. Important additional information about the role played by the different scattering channels can be gained by comparing the expressions of the SD equation after partial summations over the internal variables k', but not q, are performed.

From a physical point of view, each expression can be associated to one of the possible collective modes (e.g., density, magnetic, and singlet/triplet pairing) of the electronic system. A large contribution to the final sum over q at low transfer frequency and at a definite momentum signifies a dominant collective mode, in contrast to contributions more evenly distributed over a wide range of frequencies and momenta.

We now derive Eq. **2** in more detail. To have access to all the single- and two-particle quantities in the SD equation, we introduce the Bogoliubov–de Gennes (BdG) spinors in momentum space (28)

$$\Phi_K = \begin{pmatrix} c_{K\uparrow} & c_{K\downarrow} & c^\dagger_{-K\uparrow} & c^\dagger_{-K\downarrow} \end{pmatrix}^T. \qquad [3]$$

The single-particle Green's function in the singlet superconducting state is

$$\underline{\mathcal{G}}_K(\tau) = -\langle \mathcal{T}\Phi_K(\tau)\Phi^\dagger_K(0)\rangle \qquad [4]$$
$$= -\left\langle \mathcal{T} \begin{pmatrix} c_{K\uparrow}c^\dagger_{K\uparrow} & 0 & 0 & c_{K\uparrow}c_{K\downarrow} \\ 0 & c_{K\downarrow}c^\dagger_{K\downarrow} & c_{K\downarrow}c_{K\uparrow} & 0 \\ 0 & c^\dagger_{K\uparrow}c^\dagger_{K\downarrow} & c^\dagger_{K\uparrow}c_{K\uparrow} & 0 \\ c^\dagger_{K\downarrow}c^\dagger_{K\uparrow} & 0 & 0 & c^\dagger_{K\downarrow}c_{K\downarrow} \end{pmatrix}(\tau, 0)\right\rangle,$$

where $\mathcal{T}$ is the (imaginary) time-ordering operator. SU(2) symmetry reduces the number of independent terms in Eq. **4** to four, such that Eq. **4** can be written in a compact form as

$$\underline{\mathcal{G}}_K(\tau) = -\left\langle \mathcal{T} \begin{pmatrix} c_{K\uparrow}(\tau)c^\dagger_{K\uparrow}(0) & c_{K\uparrow}(\tau)c_{-K\downarrow}(0) \\ c^\dagger_{-K\downarrow}(\tau)c^\dagger_{K\uparrow}(0) & c^\dagger_{-K\downarrow}(\tau)c_{-K\downarrow}(0) \end{pmatrix}\right\rangle$$
$$= -\begin{pmatrix} G^N_K(\tau) & G^A_K(\tau) \\ G^{A\dagger}_K(\tau) & -G^N_{-K}(-\tau) \end{pmatrix}. \qquad [5]$$

The single-particle Green's function matrix contains both normal (N) and anomalous (A) entries, with the normal terms defined as $G^{\sigma\sigma}_K(\tau) = -\langle \mathcal{T}c_{K\sigma}(\tau)c^\dagger_{K\sigma}(0)\rangle, \sigma = \uparrow, \downarrow$, and the anomalous terms defined as $G^A_K(\tau) = G^{\uparrow\downarrow}_K(\tau) = -\langle \mathcal{T}c_{K\uparrow}(\tau)c_{-K\downarrow}(0)\rangle, G^{A\dagger}_K(\tau) = G^{\downarrow\uparrow}_K(\tau) = -\langle \mathcal{T}c^\dagger_{-K\downarrow}(\tau)c^\dagger_{K\uparrow}(0)\rangle$. Fourier transforming to frequency space and introducing shorthand notations $k = (K, i\omega_n)$, we can define $G^N_k = G^{\uparrow\uparrow}_k = G^{\downarrow\downarrow}_k$. For d-wave superconductivity on a lattice with inversion symmetry, the anomalous Green's function can be chosen to be real (29), such that $G^A_{\pm k} = G^{A\dagger}_{\pm k}$. The self-energy can then be computed with

$$\underline{\Sigma}(k) = \underline{\mathcal{G}}^{-1}_0(k) - \underline{\mathcal{G}}^{-1}(k), \qquad [6]$$

where

$$\underline{\Sigma}(k) = \begin{pmatrix} \Sigma^N_{k\uparrow} & \Sigma^A_{k\uparrow} \\ \Sigma^{A\dagger}_{k\uparrow} & -\Sigma^N_{-k\downarrow} \end{pmatrix}, \qquad [7]$$

$$\underline{\mathcal{G}}^{-1}_0(k) = \begin{pmatrix} i\omega_n - \varepsilon_k + \mu & 0 \\ 0 & i\omega_n + \varepsilon_k - \mu \end{pmatrix}. \qquad [8]$$

The two-particle Green's function takes the form

$$G^{(2)}(1234) = \langle \mathcal{T} o_1 o_2 o_3 o_4 \rangle, \quad \textbf{[9]}$$

where we use i as a shorthand notation for momentum, spin, and imaginary time indices (K_i, σ_i, τ_i). o_i is either a creation operator $c_i^\dagger$ or an annihilation operator c_i.

In the paramagnetic state, the number of creation and annihilation operators in the two-particle Green's function must be equal to preserve charge conservation. In the superconducting state, the broken U(1) symmetry gives in total $2^4 = 16$ combinations of different creation or annihilation operators, which can be written in matrix form as

$$\underline{\mathcal{G}}^{(2)}(1234) = \left\langle \mathcal{T} \begin{pmatrix} c_1^\dagger c_2 c_3^\dagger c_4 & c_1^\dagger c_2 c_3 c_4 & c_1^\dagger c_2 c_3^\dagger c_4^\dagger & c_1^\dagger c_2 c_3 c_4^\dagger \\ c_1^\dagger c_2^\dagger c_3^\dagger c_4 & c_1^\dagger c_2^\dagger c_3 c_4 & c_1^\dagger c_2^\dagger c_3^\dagger c_4^\dagger & c_1^\dagger c_2^\dagger c_3 c_4^\dagger \\ c_1 c_2 c_3^\dagger c_4 & c_1 c_2 c_3 c_4 & c_1 c_2 c_3^\dagger c_4^\dagger & c_1 c_2 c_3 c_4^\dagger \\ c_1 c_2^\dagger c_3^\dagger c_4 & c_1 c_2^\dagger c_3 c_4 & c_1 c_2^\dagger c_3^\dagger c_4^\dagger & c_1 c_2^\dagger c_3 c_4^\dagger \end{pmatrix} \right\rangle, \quad \textbf{[10]}$$

with $i = (K_i, \sigma_i, \tau_i)$, $-i = (-K_i, -\sigma_i, \tau_i)$.

Each term $G^{(2)}(1234)$ in the two-particle Green's function matrix can be decomposed into connected ($G_c^{(2)}$) and disconnected parts as

$$\begin{aligned} G_c^{(2)}(1234) = G^{(2)}(1234) &- \langle \mathcal{T} o_1 o_2 \rangle \langle \mathcal{T} o_3 o_4 \rangle \\ &+ \langle \mathcal{T} o_1 o_3 \rangle \langle \mathcal{T} o_2 o_4 \rangle - \langle \mathcal{T} o_1 o_4 \rangle \langle \mathcal{T} o_2 o_3 \rangle. \end{aligned} \quad \textbf{[11]}$$

This relation can be written in matrix form

$$\underline{\mathcal{G}}_c^{(2)}(1234) = \underline{\mathcal{G}}^{(2)}(1234) - \underline{\chi}_0^{=}(1234) - \underline{\chi}_0^{\times}(1234), \quad \textbf{[12]}$$

where $\underline{\chi}_0^{=}(1234)$ includes terms of the form $\langle \mathcal{T} o_1 o_2 \rangle \langle \mathcal{T} o_3 o_4 \rangle$, and $\underline{\chi}_0^{\times}(1234)$ includes terms of the form $\langle \mathcal{T} o_1 o_3 \rangle \langle \mathcal{T} o_2 o_4 \rangle$ and $\langle \mathcal{T} o_1 o_4 \rangle \langle \mathcal{T} o_2 o_3 \rangle$. The full vertex F can be computed from the connected part of the two-particle Green's function (30, 31)

$$G_c^{(2)}(1234) = -G(15)G(26)F(5678)G(73)G(84). \quad \textbf{[13]}$$

Due to momentum and energy conservation and following the particle-hole convention (31) of the Fourier transform, the momentum and frequency indices in the matrix above can be assigned as $k_1 = k$, $k_2 = k + q$, $k_3 = k' + q$, and $k_4 = k'$, with shorthand notations $k = (K, i\omega_n)$ for fermionic and $q = (Q, i\nu_n)$ for bosonic indices. Three spin combinations are possible in an SU(2) symmetric system, $\sigma_1 = \sigma_2 = \sigma_3 = \sigma_4$, $(\sigma_1 = \sigma_2) \neq (\sigma_3 = \sigma_4)$, and $(\sigma_1 = \sigma_4) \neq (\sigma_2 = \sigma_3)$, with $\sigma_j = \uparrow$ or $\downarrow$ (31). We can then define

$$\underline{\mathcal{G}}^{(2)}_{\sigma\sigma'}(kk'q) = \underline{\mathcal{G}}^{(2)}_{\sigma\sigma\sigma'\sigma'}(k, k+q, k'+q, k'), \quad \textbf{[14a]}$$

$$\underline{\mathcal{G}}^{(2)}_{\overline{\sigma\sigma'}}(kk'q) = \underline{\mathcal{G}}^{(2)}_{\sigma\sigma'\sigma'\sigma}(k, k+q, k'+q, k'), \quad \textbf{[14b]}$$

where quantities in Eq. **14b** can be obtained from those in Eq. **14a** via SU(2) and crossing symmetries (31). Introducing the full vertex matrix $\underline{\mathcal{F}}$, Eq. **13** can be written in matrix form as

$$\underline{\mathcal{G}}^{(2)}_{c,\sigma\sigma'}(kk'q) = -\frac{1}{\beta^2 N_c^2} \sum_{k_1 k_2} \underline{\chi}^{\times}_{0,\sigma\sigma}(kk_1q)\, \underline{\mathcal{F}}_{\sigma\sigma'}(k_1k_2q)\, \underline{\chi}^{\times}_{0,\sigma'\sigma'}(k_2k'q). \quad \textbf{[15]}$$

In order to extend fluctuation diagnostics to the superconducting state, we identify all scattering channels in the symmetry broken state and derive the corresponding equivalent expressions of the SD equation. We emphasize that the full information about all scattering processes is contained in all channels and that different channels are related by crossing relations. In the basis of BdG spinors, the creation of pairs of particles and holes in the spin singlet state is then described by the 4×4 matrices $\Sigma = (i\sigma^y) \otimes \sigma^+$, $\bar{\Sigma} = (i\sigma^y) \otimes \sigma^-$ [$\sigma^{i=x,y,z}$ being the Pauli matrices, $\sigma^\pm = \frac{1}{2}(\sigma^x \pm i\sigma^y)$], while the corresponding terms for the triplet state are given by $T = \sigma^x \otimes \sigma^+$ and $\bar{T} = \sigma^x \otimes \sigma^-$. The two 4×4 matrices $\rho = \mathbb{I}_{2\times2} \otimes \mathrm{P}_p$ and $\bar{\rho} = \mathbb{I}_{2\times2} \otimes \mathrm{P}_h$ [with $\mathrm{P}_{p(h)} = \sigma^+\sigma^-(\sigma^-\sigma^+)$ the projector in the particle (hole) subspace] define the density operator of particles and holes. Analogously, $S = \sigma^z \otimes \mathrm{P}_p$ and $\bar{S} = \sigma^z \otimes \mathrm{P}_h$ yield the spin operator, from which magnetic fluctuations originate. With these definitions, the two-particle Green's function in different physical channels can be defined as

$$G^{O_a O_b}_{KK'Q}(\tau_1, \tau_2, \tau_3, \tau_4) = \langle \mathcal{T} \hat{O}^{(a)}_{K,K+Q}(\tau_1, \tau_2) \hat{O}^{(b)}_{K'+Q,K'}(\tau_3, \tau_4) \rangle, \quad \textbf{[16]}$$

where the two time-dependent operators on the right-hand side are defined as $\hat{O}^{(a)}_{K,K+Q}(\tau_1, \tau_2) = \Phi^\dagger_K(\tau_1) \cdot O_a \cdot \Phi_{K+Q}(\tau_2)$, with O_a corresponding to one of the eight 4×4 matrices Σ, $\bar{\Sigma}$; T, $\bar{T}$; ρ, $\bar{\rho}$; S, $\bar{S}$. All terms defined by Eq. **16** can be computed from the linear combination of terms in $\underline{\mathcal{G}}^{(2)}_{c,\uparrow\uparrow}(kk'q)$ and $\underline{\mathcal{G}}^{(2)}_{c,\uparrow\downarrow}(kk'q)$.

The physical channels of the full vertex function can be defined with the same linear combinations as the two-particle Green's function. The underlying symmetries of the system block-diagonalize the 8×8 matrix $G^{O_a O_b}$, such that each block identifies one scattering channel (32). In the paramagnetic state, where both the (global) $U(1)$ symmetry and the $SU(2)$ symmetry hold, only terms that conserve spin and particle number will be nonzero (31), giving rise to four scattering channels: $\{\rho, \bar{\rho}\}$ define the density, $\{S, \bar{S}\}$ the magnetic, $\{\Sigma, \bar{\Sigma}\}$ the singlet-pairing, and $\{T, \bar{T}\}$ the triplet-pairing channels.

In the superconducting state, the spontaneously broken $U(1)$ symmetry allows for processes violating particle number conservation and mix the scattering channels found in the paramagnetic state. However, the $SU(2)$ symmetry still holds and allows us to identify two scattering channels: the density/spin-singlet channel $\{\rho, \bar{\rho}, \Sigma, \bar{\Sigma}\}$ and the magnetic/spin-triplet channel $\{S, \bar{S}, T, \bar{T}\}$. In particular, in the superconducting phase, Eq. **2** can be rewritten in two equivalent ways as

$$\Sigma^A_k = \Sigma^{A,S}_k = \Sigma^{A,\rho}_k. \quad \textbf{[17]}$$

$$\begin{aligned} \Sigma^{A,S}_k = &\frac{1}{2}\frac{U}{(\beta N_c)^2} \sum_{k'q} \left[G^N_{k+q} F_{\bar{T}S}(kk'q) G^N_{k'+q} G^N_{k'} + G^N_{k+q} F_{\bar{T}\bar{T}}(kk'q) G^N_{k'+q} G^A_{k'} \right] \\ &+ \frac{1}{2}\frac{U}{(\beta N_c)^2} \sum_{k'q} \left[G^N_{k+q} F_{\bar{T}\bar{T}}(kk'q) G^A_{k'+q} G^N_{k'} - G^N_{k+q} F_{\bar{T}\bar{S}}(kk'q) G^A_{k'+q} G^A_{k'} \right] \\ &- \frac{1}{2}\frac{U}{(\beta N_c)^2} \sum_{k'q} \left[G^A_{k+q} F_{\bar{S}S}(kk'q) G^N_{k'+q} G^N_{k'} + G^A_{k+q} F_{\bar{S}T}(kk'q) G^N_{k'+q} G^A_{k'} \right] \\ &- \frac{1}{2}\frac{U}{(\beta N_c)^2} \sum_{k'q} \left[G^A_{k+q} F_{\bar{S}\bar{T}}(kk'q) G^A_{k'+q} G^N_{k'} - G^A_{k+q} F_{\bar{S}\bar{S}}(kk'q) G^A_{k'+q} G^A_{k'} \right], \end{aligned} \quad \textbf{[18]}$$

$$\begin{aligned} \Sigma^{A,\rho}_k = &\frac{1}{2}\frac{U}{(\beta N_c)^2} \sum_{k'q} \left[G^N_{k+q} F_{\bar{\Sigma}\rho}(kk'q) G^N_{k'+q} G^N_{k'} + G^N_{k+q} F_{\bar{\Sigma}\Sigma}(kk'q) G^N_{k'+q} G^A_{k'} \right] \\ &- \frac{1}{2}\frac{U}{(\beta N_c)^2} \sum_{k'q} \left[G^N_{k+q} F_{\bar{\Sigma}\bar{\Sigma}}(kk'q) G^A_{k'+q} G^N_{k'} - G^N_{k+q} F_{\bar{\Sigma}\bar{\rho}}(kk'q) G^A_{k'+q} G^A_{k'} \right] \\ &- \frac{1}{2}\frac{U}{(\beta N_c)^2} \sum_{k'q} \left[G^A_{k+q} F_{\bar{\rho}\rho}(kk'q) G^N_{k'+q} G^N_{k'} + G^A_{k+q} F_{\bar{\rho}\Sigma}(kk'q) G^N_{k'+q} G^A_{k'} \right] \\ &+ \frac{1}{2}\frac{U}{(\beta N_c)^2} \sum_{k'q} \left[G^A_{k+q} F_{\bar{\rho}\bar{\Sigma}}(kk'q) G^A_{k'+q} G^N_{k'} - G^A_{k+q} F_{\bar{\rho}\bar{\rho}}(kk'q) G^A_{k'+q} G^A_{k'} \right]. \end{aligned} \quad \textbf{[19]}$$

Eqs. **18** and **19** are the decompositions that enable application of the fluctuation diagnostics scheme to the superconducting state.

Results

Fig. 2 gives the phase diagram of the two-dimensional Hubbard model on the hole-doped side within the DCA approximation at intermediate interaction strength (18) showing the pseudogap, superconducting, and metallic regimes. The pseudogap regime is characterized by a suppression of the single-particle spectral function, and the superconducting phase corresponds to the region

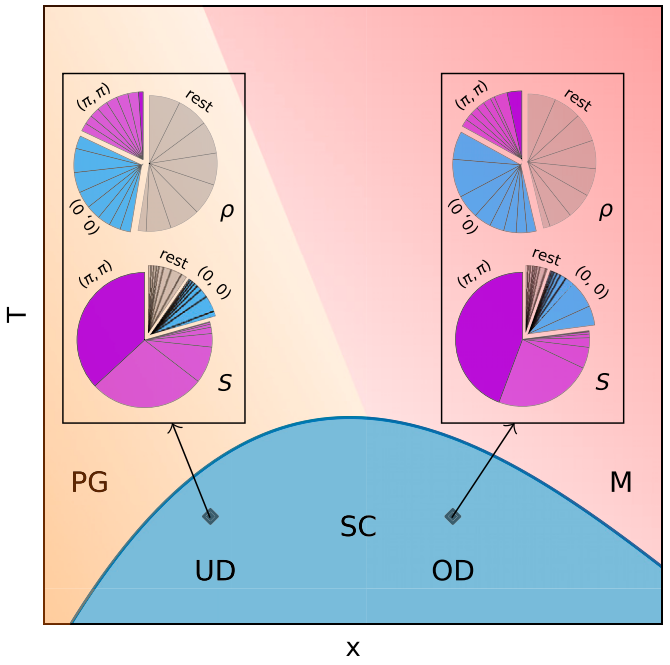

Fig. 2. Phase diagram sketch, with pseudogap (PG; orange), metal (M; red), and superconducting (SC; blue) regimes. Black diamonds denote UD and OD data points analyzed in detail. (*Inset*) Pie chart of $|\mathrm{Re}\Sigma^A_{(\pi,0),Q\nu}(i\omega_0)|$ in the density (ρ) and magnetic (S) channels. Counterclockwise from the top, pieces represent contributions for momentum $Q=(\pi,\pi)$, $Q=(0,0)$ and summation over the remaining momenta in an eight-site cluster. In each slice, separation indicates bosonic frequency ν_n with $n=0,\pm1,\ldots\pm7$.

where the anomalous Green's function is nonzero. We present the results for two representative parameter sets without next-nearest neighbor hopping on an eight-site cluster with $U=6t$, $\beta t=45$, i.e., $x=0.031$ ($T_c\in(t/30,t/35]$, corresponding to underdoped (UD) for this value of U) and $x=0.075$ ($T_c\in(t/30,t/35]$, corresponding to overdoped (OD) for this value of U); see ref. 18 for a phase diagram. In DCA, both cases considered lie deep in the superconducting phase where the anomalous Green's function G^A_k is nonzero for $K=(0,\pi)$ and $(\pi,0)$, with relation $G^A_{(0,\pi)}=-G^A_{(\pi,0)}$. Cluster momentum points are shown in Fig. 3, *Inset*. Fig. 2, *Inset*, shows the momentum (Q) and frequency (ν_n) distribution of $|\mathrm{Re}\Sigma^A_{(\pi,0),Q\nu}(i\omega_0)|$, which is computed by summing over fermionic indices k' but not over q in Eqs. **18** and **19**. The pie chart insets show that for both UD and OD, there is a dominant contribution from $Q=(\pi,\pi)$ and $\nu_n=0$ in the magnetic/triplet channel S. In the density/singlet channel ρ, contributions from different momenta and frequencies are evidently distributed much more evenly.

We first focus on the momentum distribution of $\mathrm{Re}\Sigma^A_{(\pi,0),Q}(i\omega_n)$ within the two physical channels in Fig. 3, computed by summing over all indices in Eqs. **18** and **19** except for the transferred momentum Q. Fig. 3, *Upper Left*, *Inset*, shows the momentum points in an eight-site cluster and the Fermi surface in the noninteracting system for dopings of 0.2 (corresponding to hole doping), 0, −0.2, and −0.4 (corresponding to electron doping). Fig. 3, *Left*, shows the contribution of different Q in the density channel. The weak Q dependence indicates the absence of a dominant mode in this channel. Results for the magnetic/triplet channel are shown in Fig. 3, *Right*. The transfer momentum $Q=(\pi,\pi)$ associated with antiferromagnetic (AFM) fluctuations is clearly the dominant mode in both the UD and the OD regime. We note that a subleading, although still sizable, negative contribution to the anomalous self-energy is originated by a ferromagnetic mode with $Q=(0,0)$. The black lines with crosses are computed by summing over all different momenta in the cluster, resulting in $\Sigma^{A,S}$ and $\Sigma^{A,\rho}$ of Eq. **17**.

Important insight can be gained by a complementary analysis in frequency space: Fig. 4 shows the frequency dependence of $\mathrm{Re}\Sigma^A_{(\pi,0),\nu_n}(i\omega_0)$, corresponding to the result at the lowest fermionic Matsubara frequency $i\omega_0=\pi/\beta$ after summation over all indices except for bosonic frequency ν_n in Eqs. **18** and **19**. The low-frequency peak in the magnetic channel identifies the corresponding fluctuation as a well-defined and long-lived mode. In the density representation, the same fluctuations are short range and short lived. This indicates that the density representation is not suitable for a simple interpretation of the superconducting mechanism.

Discussion and Conclusion

By extending the fluctuation diagnostics approach to the superconducting phase, we have been able to unambiguously identify spin fluctuations (1–4) as the dominant contribution to the d-wave pairing in the Hubbard model at interaction strengths believed to be relevant for the cuprates, i.e., beyond the weak-coupling regime (1, 6, 8, 9). At the same time, consistent with the existing work in the normal state (14, 33, 34), we do not find any indication supporting the alternative scenarios mentioned in the Introduction, such as nematic fluctuations (11), loop current order (12), or intertwining of different orders (13). In order for these scenarios to become relevant in larger systems or in other areas of parameter space, superconductivity from spin fluctuations would have to disappear while new mechanisms would

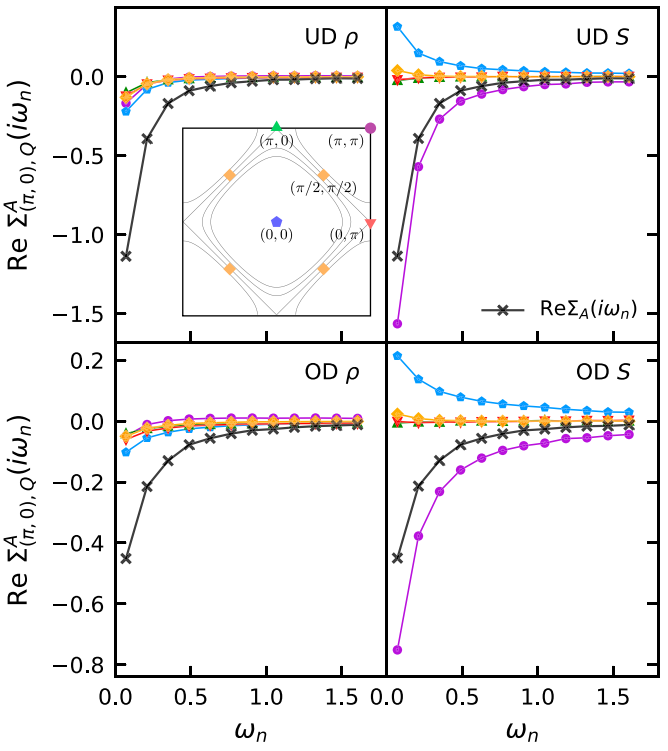

Fig. 3. $\mathrm{Re}\Sigma^A_{(\pi,0),Q}(i\omega_n)$ for several transfer momenta Q in the density (ρ) and magnetic (S) channels. OD and UD correspond to the diamonds in Fig. 2. Black line with crosses indicates total anomalous self-energy after summation over all Q. (*Inset*) Noninteracting Fermi surface and location of momentum points corresponding to colors in main panels. $\omega_n=(2n+1)\pi T$ indicates fermionic Matsubara frequency. *Top Left*: UD, ρ. *Top Right*: UD, S. *Bottom Left*: OD, ρ. *Bottom Right*: OD, S.

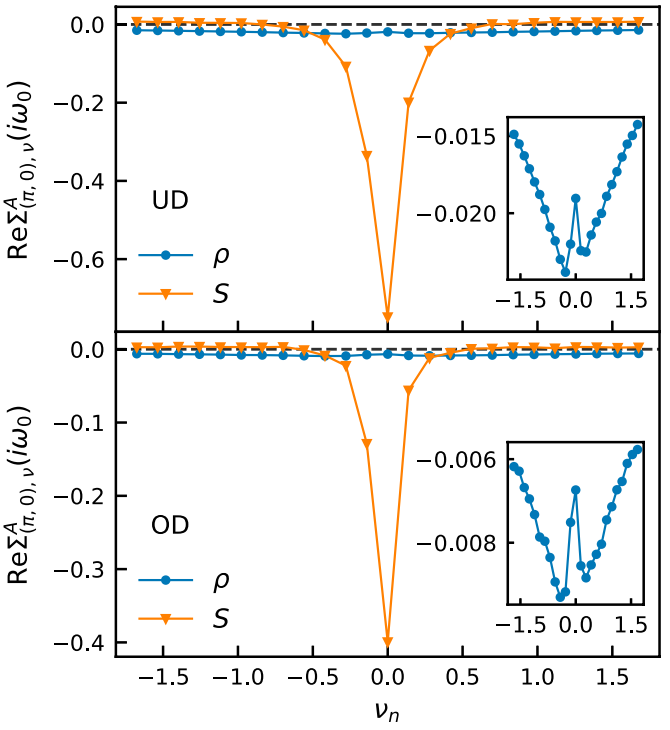

Fig. 4. $\mathrm{Re}\Sigma^{A}_{(\pi,0),\nu}(i\omega_0)$ in density (ρ) and magnetic (S) channels. OD and UD correspond to the two data points of Fig. 2. (*Inset*) $\mathrm{Re}\Sigma_{A,\nu}(i\omega_0)$ in density channel with rescaled y axis. $\nu_n = 2n\pi T$ indicates bosonic Matsubara frequency. *Top*: UD. *Bottom*: OD.

have to emerge simultaneously, which we believe to be exceedingly unlikely. In the case of intertwined orders, multiple fluctuations such as density or magnetic ones would contribute synergistically to the pairing, rather than compete, in contradiction with our results. We emphasize that the fluctuation diagnostic is capable of detecting the occurrence of this situation, when it is realized, e.g., in the attractive Hubbard model (14).

Our identification of the superconducting glue agrees with the findings of several experiments. Ref. 35 finds good quantitative agreement between the spectral function computed from conventional spin fluctuation theory with magnetic susceptibility measured by inelastic neutron scattering and the spectral function measured from angle-resolved photoemission spectroscopy in the superconducting phase of $YBa_2Cu_3O_{6.6}$. Inelastic photon scattering experiments (36) on Hg1201 and Hg1212 infer that the superconducting temperature T_c can be determined by the strength of the magnetic interactions (paramagnon signals), supporting the theory of magnetically mediated high-temperature superconductivity. Other experiments suggest a relation between superconductivity and charge density wave (37) or that the pseudogap and superconductivity may have different origins (38). Thus, the numerical findings of our study suggest the possibility that the latter class of experiments may be probing aspects of cuprates physics beyond those encoded in the single-orbital Hubbard model on an eight-site DCA cluster.

Independently of the agreement with this multifaceted experimental evidence, our identification of the superconducting glue in terms of spin fluctuations touches a delicate and important aspect of the theoretical description of high-T superconductivity. In particular, conventional spin fluctuation theory (39–44) appears only able to capture a fraction of the pairing contribution (44) or overestimate the results (42), depending on the analysis procedure used. The origin of this discrepancy can be ascribed to the random phase approximation-like spin fluctuation expressions used in conventional approaches which, outside of the weak-coupling regime, do not capture all spin fluctuation–mediated processes (45).

The microscopic picture of superconductivity emerging from our analysis agrees well with recent studies of the description of the nonsuperconducting pseudogap regime: while spin fluctuations were identified as the predominant mechanism of the pseudogap (14, 33, 34), differences with respect to the predictions of conventional spin fluctuation theory were found and traced (46) to the imaginary part of the dynamical scattering amplitude between electrons and spin fluctuations, which is absent in conventional approaches (46).

In conclusion, our fluctuation diagnostics of the superconducting order in the Hubbard model precisely identify antiferromagnetic spin fluctuations as the glue of the d-wave pairing. This conclusion applies to the intermediate-to-large values of the electronic interaction relevant to cuprate physics. For this reason, the spin fluctuation–driven pairing found in our calculations is expected to differ from conventional spin fluctuation theories.

Data Availability. Due to the prohibitively large size of the files, the datasets generated during the current study and the computer codes for data analysis are available upon request.

ACKNOWLEDGMENTS. XD and EG are supported by NSF DMR 2001465. L.D. acknowledges financial support from the U.S. Department of Energy, Office of Science, Basic Energy Sciences, Division of Materials Sciences and Engineering under Grant No. DE-SC0019469. A.T. acknowledges financial support from the Austrian Science Fund (FWF) through the Project I 5868 (part of the FOR 5249 [QUAST] of the German Research Foundation, DFG). We thank A.J. Millis, Kai Sun and F. Krien for detailed and insightful discussions.

1. D. J. Scalapino, E. Loh Jr., J. E. Hirsch, *d*-wave pairing near a spin-density-wave instability. *Phys. Rev. B Condens. Matter* **34**, 8190–8192 (1986).
2. K. Miyake, S. Schmitt-Rink, C. M. Varma, Spin-fluctuation-mediated even-parity pairing in heavy-fermion superconductors. *Phys. Rev. B Condens. Matter* **34**, 6554–6556 (1986).
3. D. J. Scalapino, Superconductivity and spin fluctuations. *J. Low Temp. Phys.* **117**, 179–188 (1999).
4. D. J. Scalapino, A common thread: The pairing interaction for unconventional superconductors. *Rev. Mod. Phys.* **84**, 1383–1417 (2012).
5. C. J. Halboth, W. Metzner, *d*-wave superconductivity and pomeranchuk instability in the two-dimensional Hubbard model. *Phys. Rev. Lett.* **85**, 5162–5165 (2000).
6. D. Zanchi, H. J. Schulz, Weakly correlated electrons on a square lattice: Renormalization-group theory. *Phys. Rev. B Condens. Matter Mater. Phys.* **61**, 13609–13632 (2000).
7. C. Honerkamp, M. Salmhofer, N. Furukawa, T. M. Rice, Breakdown of the Landau-Fermi liquid in two dimensions due to umklapp scattering. *Phys. Rev. B Condens. Matter Mater. Phys.* **63**, 035109 (2001).
8. S. Raghu, S. A. Kivelson, D. J. Scalapino, Superconductivity in the repulsive Hubbard model: An asymptotically exact weak-coupling solution. *Phys. Rev. B Condens. Matter Mater. Phys.* **81**, 224505 (2010).
9. Y. Deng, E. Kozik, N. V. Prokof'ev, B. V. Svistunov, Emergent BCS regime of the two-dimensional fermionic Hubbard model: Ground-state phase diagram. *Europhys. Lett.* **110**, 57001 (2015).
10. P. W. Anderson, The resonating valence bond state in La_2CuO_4 and superconductivity. *Science* **235**, 1196–1198 (1987).
11. E. Fradkin, S. A. Kivelson, M. J. Lawler, J. P. Eisenstein, A. P. Mackenzie, Nematic Fermi fluids in condensed matter physics. *Annu. Rev. Condens. Matter Phys.* **1**, 153–178 (2010).
12. A. Allais, T. Senthil, Loop current order and *d*-wave superconductivity: Some observable consequences. *Phys. Rev. B Condens. Matter Mater. Phys.* **86**, 045118 (2012).
13. E. Fradkin, S. A. Kivelson, J. M. Tranquada, Colloquium: Theory of intertwined orders in high temperature superconductors. *Rev. Mod. Phys.* **87**, 457–482 (2015).
14. O. Gunnarsson *et al.*, Fluctuation diagnostics of the electron self-energy: Origin of the pseudogap physics. *Phys. Rev. Lett.* **114**, 236402 (2015).
15. T. Maier, M. Jarrell, T. Pruschke, M. H. Hettler, Quantum cluster theories. *Rev. Mod. Phys.* **77**, 1027–1080 (2005).
16. E. Gull, P. Werner, O. Parcollet, M. Troyer, Continuous-time auxiliary-field Monte Carlo for quantum impurity models. *Europhys. Lett.* **82**, 57003 (2008).
17. E. Gull *et al.*, Continuous-time Monte Carlo methods for quantum impurity models. *Rev. Mod. Phys.* **83**, 349–404 (2011).
18. E. Gull, O. Parcollet, A. J. Millis, Superconductivity and the pseudogap in the two-dimensional Hubbard model. *Phys. Rev. Lett.* **110**, 216405 (2013).
19. X. Chen, J. P. F. LeBlanc, E. Gull, Superconducting fluctuations in the normal state of the two-dimensional Hubbard model. *Phys. Rev. Lett.* **115**, 116402 (2015).
20. B. X. Zheng *et al.*, Stripe order in the underdoped region of the two-dimensional Hubbard model. *Science* **358**, 1155–1160 (2017).

21. E. W. Huang, C. B. Mendl, H. C. Jiang, B. Moritz, T. P. Devereaux, Stripe order from the perspective of the Hubbard model. *npj Quantum Mater.* **3**, 22 (2018).
22. M. Qin *et al.*, Absence of superconductivity in the pure two-dimensional Hubbard model. *Phys. Rev. X* **10**, 031016 (2020).
23. P. Mai, S. Karakuzu, G. Balduzzi, S. Johnston, T. A. Maier, Intertwined spin, charge, and pair correlations in the two-dimensional Hubbard model in the thermodynamic limit. *Proc. Natl. Acad. Sci. U.S.A.* **119**, e2112806119 (2022).
24. A. Wietek, Y. Y. He, S. R. White, A. Georges, E. M. Stoudenmire, Stripes, antiferromagnetism, and the pseudogap in the doped Hubbard model at finite temperature. *Phys. Rev. X* **11**, 031007 (2021).
25. F. Šimkovic, R. Rossi, M. Ferrero, The weak, the strong and the long correlation regimes of the two-dimensional Hubbard model at finite temperature. arXiv [Preprint] (2021). https://arxiv.org/abs/2110.05863 (Accessed 2 August 2022).
26. G. Rohringer, Spectra of correlated many-electron systems: From a one- to a two-particle description. *J. Electron Spectrosc. Relat. Phenom.* **241**, 146804 (2020).
27. T. Schäfer, A. Toschi, How to read between the lines of electronic spectra: The diagnostics of fluctuations in strongly correlated electron systems. *J. Phys. Condens. Matter* **33**, 214001 (2021).
28. J. Zhu, *Bogoliubov-de Gennes Method and Its Applications.* (Springer, 2016). https://link.springer.com/book/10.1007/978-3-319-31314-6. Accessed 2 August 2022.
29. A. I. Lichtenstein, M. I. Katsnelson, Antiferromagnetism and d-wave superconductivity in cuprates: A cluster dynamical mean-field theory. *Phys. Rev. B Condens. Matter Mater. Phys.* **62**, R9283–R9286 (2000).
30. J. Negele, H. Orland, *Quantum Many-Particle Systems.* DOI: 10.1201/9780429497926. (Taylor & Francis, 1998).
31. G. Rohringer, A. Valli, A. Toschi, Local electronic correlation at the two-particle level. *Phys. Rev. B Condens. Matter Mater. Phys.* **86**, 125114 (2012).
32. L. Del Re, A. Toschi, Dynamical vertex approximation for many-electron systems with spontaneously broken SU(2) symmetry. *Phys. Rev. B* **104**, 085120 (2021).
33. W. Wu, M. Ferrero, A. Georges, E. Kozik, Controlling Feynman diagrammatic expansions: Physical nature of the pseudogap in the two-dimensional Hubbard model. *Phys. Rev. B* **96**, 041105 (2017).
34. X. Dong, X. Chen, E. Gull, Dynamical charge susceptibility in the Hubbard model. *Phys. Rev. B* **100**, 235107 (2019).
35. T. Dahm *et al.*, Strength of the spin-fluctuation-mediated pairing interaction in a high-temperature superconductor. *Nat. Phys.* **5**, 217–221 (2009).
36. L. Wang *et al.*, Paramagnons and high-temperature superconductivity in a model family of cuprates. *Nat. Commun.* **13**, 3163 (2022).
37. H. Chu *et al.*, Fano interference of the Higgs mode in cuprate high-Tc superconductors. arXiv [Preprint] (2021). https://arxiv.org/abs/2109.09971 (Accessed 22 October 2021).
38. Z. B. Wu *et al.*, Homogeneous superconducting gap in $Dyba_2cu_3o_{7-\delta}$ synthesized by oxide molecular beam epitaxy. *Phys. Rev. Mater.* **4**, 124801 (2020).
39. T. A. Maier, M. S. Jarrell, D. J. Scalapino, Structure of the pairing interaction in the two-dimensional Hubbard model. *Phys. Rev. Lett.* **96**, 047005 (2006).
40. T. A. Maier, M. Jarrell, D. J. Scalapino, Spin susceptibility representation of the pairing interaction for the two-dimensional Hubbard model. *Phys. Rev. B Condens. Matter Mater. Phys.* **75**, 134519 (2007).
41. T. A. Maier, D. Poilblanc, D. J. Scalapino, Dynamics of the pairing interaction in the Hubbard and $t-j$ models of high-temperature superconductors. *Phys. Rev. Lett.* **100**, 237001 (2008).
42. T. A. Maier *et al.*, Pairing in a dry Fermi sea. *Nat. Commun.* **7**, 11875 (2016).
43. T. A. Maier, D. J. Scalapino, Pairfield fluctuations of a 2D Hubbard model. *npj Quantum Mater.* **4**, 30 (2019).
44. X. Dong, E. Gull, A. J. Millis, Quantifying the role of antiferromagnetic fluctuations in the superconductivity of the doped Hubbard model. arXiv [Preprint] (2022). https://arxiv.org/abs/2202.10577 (Accessed 11 March 2022).
45. M. Kitatani, T. Schäfer, H. Aoki, K. Held, Why the critical temperature of high-T_c cuprate superconductors is so low: The importance of the dynamical vertex structure. *Phys. Rev. B* **99**, 041115 (2019).
46. F. Krien, P. Worm, P. Chalupa, A. Toschi, K. Held, Spin scattering turns complex at strong coupling: The key to pseudogap and fermi arcs in the Hubbard model. arXiv [Preprint] (2021). https://arxiv.org/abs/2107.06529 (Accessed 14 July 2021).